Paajanen, Antti; Zitting, Aleksi; Rautkari, Lauri; Ketoja, Jukka A.; Penttilä, Paavo A.

Nanoscale Mechanism of Moisture-Induced Swelling in Wood Microfibril Bundles

Published in:
Nano Letters

DOI:
10.1021/acs.nanolett.2c00822

Published: 13/07/2022

Document Version
Publisher's PDF, also known as Version of record

NANO LETTERS

pubs.acs.org/NanoLett

Letter

Nanoscale Mechanism of Moisture-Induced Swelling in Wood Microfibril Bundles

Antti Paajanen,* Aleksi Zitting, Lauri Rautkari, Jukka A. Ketoja, and Paavo A. Penttilä*

Cite This: *Nano Lett.* 2022, 22, 5143−5150

Read Online

ACCESS | Metrics & More | Article Recommendations | Supporting Information

ABSTRACT: Understanding nanoscale moisture interactions is fundamental to most applications of wood, including cellulosic nanomaterials with tailored properties. By combining X-ray scattering experiments with molecular simulations and taking advantage of computed scattering, we studied the moisture-induced changes in cellulose microfibril bundles of softwood secondary cell walls. Our models reproduced the most important experimentally observed changes in diffraction peak locations and widths and gave new insights into their interpretation. We found that changes in the packing of microfibrils dominate at moisture contents above 10−15%, whereas deformations in cellulose crystallites take place closer to the dry state. Fibrillar aggregation is a significant source of drying-related changes in the interior of the microfibrils. Our results corroborate the fundamental role of nanoscale phenomena in the swelling behavior and properties of wood-based materials and promote their utilization in nanomaterials development. Simulation-assisted scattering analysis proved an efficient tool for advancing the nanoscale characterization of cellulosic materials.

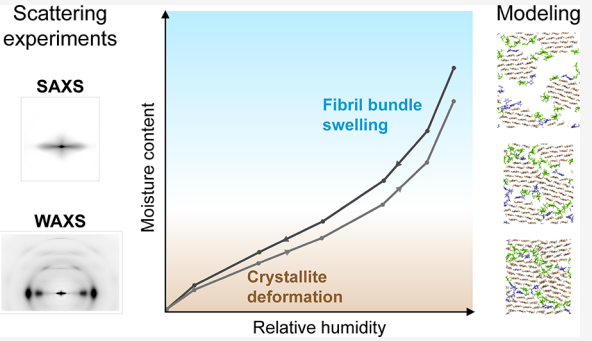

KEYWORDS: *Wood-water interactions, Cell wall nanostructure, Cellulose crystallinity, X-ray scattering, Molecular dynamics*

The intriguing characteristics of natural and engineered wood arise from their nanoscale structure, in which water is a key component.[1−5] Utilization of wood in engineering applications or as a renewable polymer source for advanced materials would benefit from a detailed picture of its structural organization at varied moisture conditions.[6−9] Furthermore, exploitation of the interactions between cellulose nanostructure and water could enable entirely new nanotechnological applications.[10−12]

The structure of wood is highly hierarchical (Figure 1), consisting of elongated fibrillar structures at all levels. The most important structural level is that of cellulose microfibrils. Their organization directly affects various properties of wood from mechanical behavior to susceptibility to chemical and enzymatic treatments, and eventually to the properties of cellulose-based nanomaterials.[3,13−15] In the secondary cell walls of wood, microfibrils consisting of parallel cellulose chains are bundled together with hemicelluloses and lignin. The exact molecular-level architecture of the microfibril bundles and the role of water as a structural component are still under active research.[16−18] A major challenge is the rarity of experimental methods for characterization of the wood nanostructure under various external conditions.[19]

X-ray and neutron scattering enable real-time and non-invasive characterization of wood across multiple length scales and under varying conditions. Results obtained with small-angle X-ray and neutron scattering (SAXS, SANS) show that the distance between microfibrils increases and the microfibril bundles swell with increasing moisture content and vice versa while drying.[20−23] Wide-angle X-ray scattering (WAXS) and X-ray diffraction studies of wood and other cellulosic materials have shown changes in the positions and widths of the diffraction peaks from crystalline cellulose, although the exact mechanism behind the observed changes is still unclear.[24−33]

A more detailed picture of molecular level phenomena can be obtained by computer simulations.[34] Atomistic simulations can help explain and visualize scattering results and provide information on the molecular organization within the microfibril bundles. Simulation studies addressing plant cell wall nanostructure have identified different stages in the moisture-induced swelling of wood cell walls, which agree for instance with sorption data.[35,36] However, a direct link to experimentally observed nanostructural changes in real wood samples has been missing.

The present work combines in situ scattering experiments with atomistic simulations and takes advantage of scattering intensities computed from the simulated structures. This approach allows direct comparison between the modeling and

Received: February 28, 2022
Revised: June 21, 2022
Published: June 29, 2022

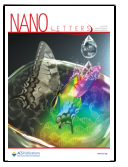

https://doi.org/10.1021/acs.nanolett.2c00822
Nano Lett. 2022, 22, 5143−5150

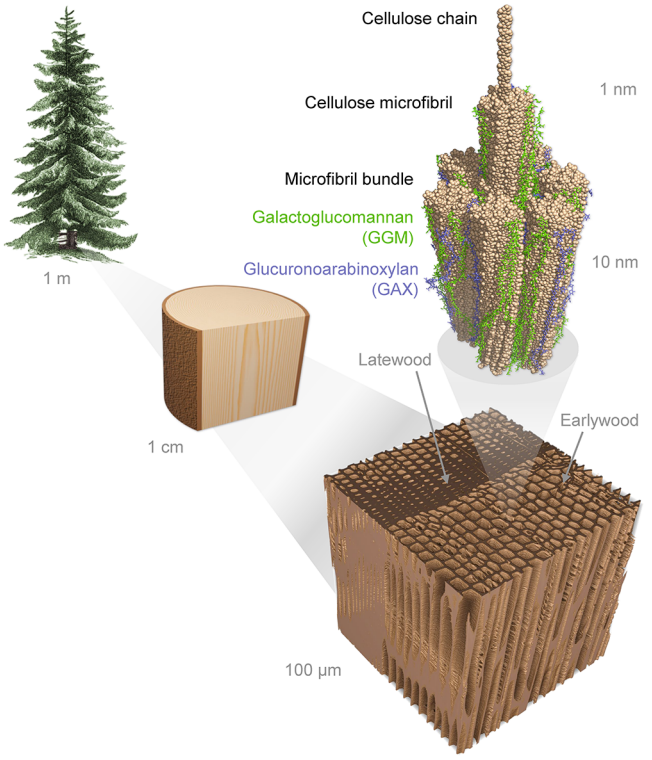

Figure 1. Cartoon representation of the hierarchical structure of spruce wood. The wood tissue (bottom right) consists of elongated tracheid cells, whose secondary cell walls bear the load of the tree. Cellulose microfibril bundles (top right) that consist of microfibrils with a diameter of 2−3 nm are a central component of the secondary cell wall structure. Lignin domains between microfibril bundles are not depicted.

experimental results, and the models visualize the effects detected in scattering experiments.[37] We have now been able to relate changes in the molecular and microfibril structures to moisture changes in wood cell walls. Our results provide a more concrete and cohesive picture of the nanoscale moisture behavior of wood, which is crucial to understand its properties and processability. It thus enables a more developed utilization of wood for nanotechnological and other applications.

We conducted SAXS/WAXS experiments on never-dried spruce wood (*Picea abies*) in controlled moisture conditions (Figure 2a−c).[38] The measurement was done first in fully wet state and subsequently at relative humidity (RH) levels from 95% to 10% and back (Figure S1 in Supporting Information (SI)). The strong orientation of wood nanostructure results in anisotropic X-ray scattering patterns (insets in Figure 2a), which allows separation of diffraction peaks from different directions in the crystal lattice. The isotropic scattering component can be subtracted (Figure S2) to obtain specific structural information perpendicular (equatorial) or parallel (meridional) to the longitudinal axis of the microfibrils. The moisture content (MC), defined as the mass ratio of water and the dry sample, at different RHs was determined by separate gravimetric measurements, and the value 41% for water-saturated cell walls was taken from literature.[39] The sample contained 44% cellulose, 17% galactoglucomannan (GGM), 7% glucuronoarabinoxylan (GAX), and 27% lignin, as measured by dry weight (Table S1), and 43% latewood by cell wall volume, determined with X-ray microtomography (Figure S5).

To relate our experimental observations to real-space molecular configurations, we conducted molecular dynamics (MD) simulations of microfibril bundles under various moisture conditions (see Figure S3). A periodic system of four microfibrils in a hexagonal arrangement (Figure 2d) was simulated with precise control of MC, and a non-periodic bundle of seven microfibrils was used complementarily. In addition, results from a periodic model of one microfibril are presented in the SI (see Figure S3 for all models). The models were built of cellulose microfibrils consisting of 18 cellulose chains[40] initially in the cellulose I_β crystal lattice,[41] with 2-3-4-4-3-2 parallel chains in each hydrogen-bonded layer[42] and no extensive disordered regions along the fibril length.[43] In the non-periodic models, the fibrils could twist around their long axis, whereas in the periodic models the fibrils were fixed by boundary constraints. The cellulose fibrils were coated by GGM and GAX chains, with their proportions reflecting the chemical composition of the wood sample (Table S1) and following the recently outlined molecular architecture of spruce wood.[17] Water was able to penetrate the hemicellulose matrix between the microfibrils and to induce swelling of the aggregate (SI video). As a preliminary test of the models' feasibility, we confirmed that the predicted mass density and microfibril packing distance at different MCs were consistent with typical values of the cell wall density (Figure S6) and small-angle scattering results from the literature.[20−23,44]

To enable direct comparison between the simulation and scattering results and to gain insight into their interpretation, we computed scattering intensities based on the atomistic models (Figure 2e,f). The calculation was performed microfibril-by-microfibril, that is, by separating individual microfibrils from the bundles and treating them as single scatterers, assuming random orientation around the fibril axis.[45] This yielded scattering intensities comparable to the equatorial and meridional anisotropic intensities from the SAXS/WAXS experiments. To study the contribution of hemicelluloses to the scattering, the intensities were also computed without the hemicelluloses. Scattering from a complete non-periodic bundle of seven fibrils was computed to illustrate the effect of microfibril aggregation. The WAXS intensities exhibited the cellulose I_β diffraction pattern, whereas the artificial lack of cell wall material around the fibrils introduced strong oscillations to the intensity in the SAXS range, that is, at values of the scattering vector q below 0.8 Å^{-1}.

Perhaps the simplest fundamental information available from WAXS data of crystalline cellulose are the lattice spacings (d_{hkl}), which are related to the locations of the diffraction peaks (with Miller indices hkl) in the reciprocal space (described by scattering vector $\mathbf{q}$). The anisotropic WAXS intensities showed clear changes in the positions of the diffraction peaks (Figures 2b,c, S8). As the sample dried, the shifts of the most intense diffraction peaks (hkl = 200 and 004) indicated an increase in the lattice spacing perpendicular to the hydrogen-bonded layers (d_{200}) and a decrease along the fibril axis (d_{004}) and partial recovery when increasing the RH again (Figure S8c). The incomplete recovery with respect to RH is related to the commonly known sorption hysteresis of wood (difference between adsorption and desorption isotherms).[2] When examined against the actual MC of the samples, a reversible trend is revealed (Figure 3a). The experimental results agreed well with lattice spacings determined directly from the models (Figure 3a). In addition, the models showed that the variation of d_{200} and d_{004} was larger close to the microfibril surfaces and increased at lower MCs (Figure S9). Only the absolute level of d_{004} deviated from the experiments, which is characteristic of the force field used in the simulations (GLYCAM06)[46] and also

https://doi.org/10.1021/acs.nanolett.2c00822
Nano Lett. 2022, 22, 5143−5150

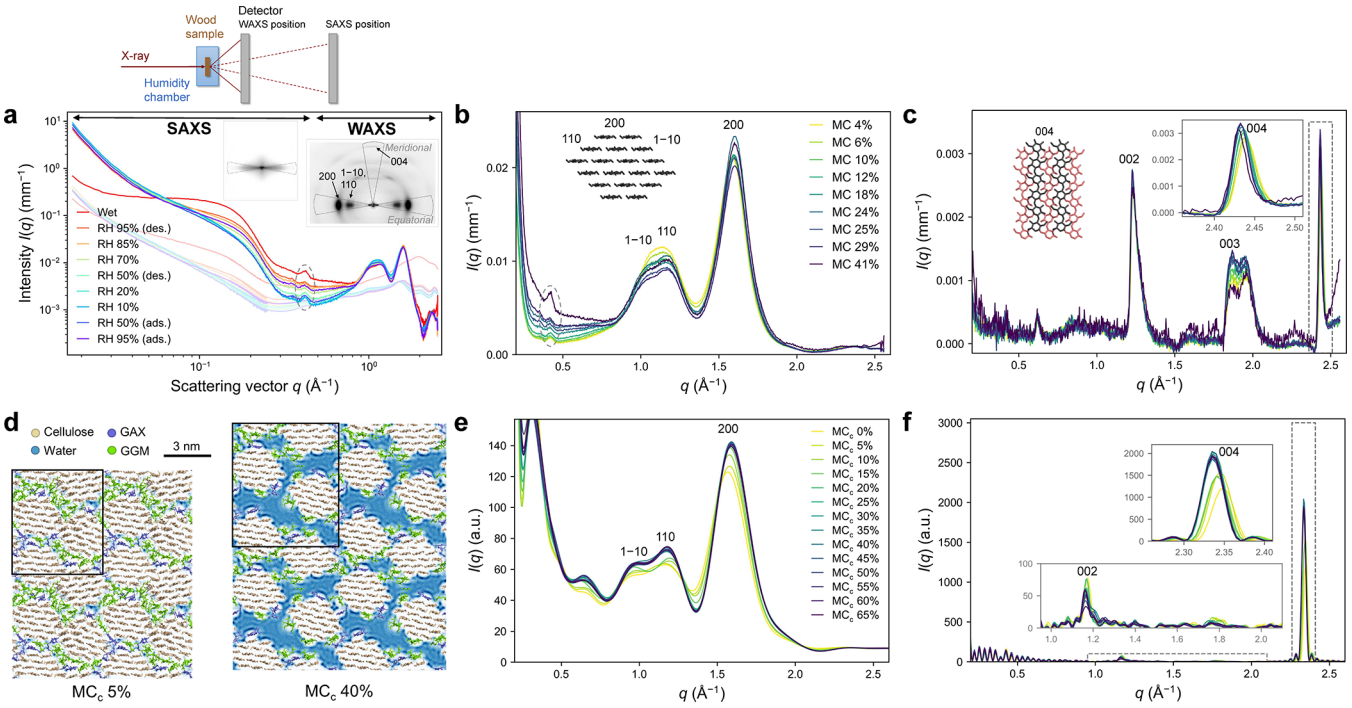

Figure 2. X-ray scattering at different moisture conditions, as observed experimentally (a–c) and computed (e,f) from molecular models such as in (d). (a) Equatorial anisotropic SAXS and WAXS intensities on double-logarithmic axes with the isotropic scattering contribution shown with light-colored lines. A schematic representation of the experiment is shown above the image. The main reflections from cellulose I_β and the equatorial and meridional integration sectors are indicated in the two-dimensional scattering patterns shown as insets. (b) Equatorial and (c) meridional anisotropic WAXS intensities, labeled with the corresponding moisture content (MC). The peak marked by a dashed line in (a) and (b) is due to unsuccessful background subtraction (Kapton windows), see SI for details. (d) Molecular model of a microfibril bundle of four microfibrils in a periodic simulation domain (domain outlined in black). MC_c refers to the moisture content relative to the carbohydrates. (e) Equatorial and (f) meridional scattering intensities computed fibril-by-fibril from the model shown in (d), excluding water, labeled with the MC_c (see Figure S7 for scattering intensities computed from all models).

attributable to the natural variation of d_{004}, possibly due to residual growth stresses.[18] When fitting the computed intensities in the same way as the experimental WAXS data (Figures 3a, S10), the expected behavior was found for d_{200} and d_{004}.

Changes in the diagonal directions of the microfibril cross-section ($d_{1\bar{1}0}$ and d_{110}) were less systematic (Figure 3b). The experiments indicated a decrease in both with drying, whereas $d_{1\bar{1}0}$ in the models showed a change in the opposite direction and d_{110} remained rather constant. In the models, these lattice spacings were sensitive to the specific aggregation of the microfibrils, and similar to d_{200} and d_{004} their variations were strongest on the microfibril surfaces and increased towards the dry state (Figure S9). In the computed scattering intensities, fits to the $1\bar{1}0$ and 110 peaks often reflected the changes in lattice spacings determined directly from the models (Figures 3b, S10, and S11a). When examining the results as lattice parameters of the monoclinic unit cell, the largest discrepancies between the experimental and model-based results were found in the lattice constant b (in the hydrogen-bonded layer, perpendicular to the chain axis) and the monoclinic angle γ (Figure S11b). These observations indicate that the $1\bar{1}0$ and 110 diffraction peaks are sensitive to the molecular configurations at microfibril surfaces and fibrillar aggregation,[47] which thus contribute to the WAXS analysis of cellulosic samples.

In the experimental WAXS data (Figures 2b,c), the diffraction peaks broadened with drying. Such broadening can originate from increased variation of the lattice spacings or a decrease in the coherence length of the crystalline order (crystal size). As both interpretations relate broader peaks with less ordered structure, we discuss the peak broadening using the term "crystal size", L_{hkl}, which is inversely proportional to the peak width after correcting for instrument-related broadening (SI eq S2). The parameter L_{hkl} decreased with drying for all peaks in the experimental WAXS data and for most peaks in the intensities computed from most models (Figures 3c,d, S10). The $1\bar{1}0$ peak in the computed scattering intensities showed an opposite trend, which could be an effect of the SAXS-range oscillations disturbing the fitting. By comparing the crystal size L_{200} computed from the same model either including or excluding the scattering from hemicelluloses (Figure 3c), a contribution of 0.2 nm to the crystal size can be attributed to the hemicelluloses. The peak broadening and crystal size are therefore sensitive to changes in the organization of hemicelluloses on the microfibril surfaces, which varied with MC in the molecular models. However, the observed broadening of the modeling-based lattice spacing distributions with drying (Figure S9) suggests that the experimental WAXS peak broadening could be largely due to a drying-induced distortion of the crystal structure.

Various explanations have been suggested for the shifts of diffraction peaks with moisture,[26,27,30−33,48] and their compatibility with our modeling results is discussed in Table S2. Our conclusion is that although the drying of the matrix polymers (hemicelluloses) may introduce compressive forces especially along the fibril,[24] the most significant deformations of the crystallites at low MCs should originate from an overall reorganization of the interfibrillar matrix and fibrillar aggregation. This explanation is supported by visual inspection of the models, where the surfaces of the microfibrils become especially

https://doi.org/10.1021/acs.nanolett.2c00822
Nano Lett. 2022, 22, 5143−5150

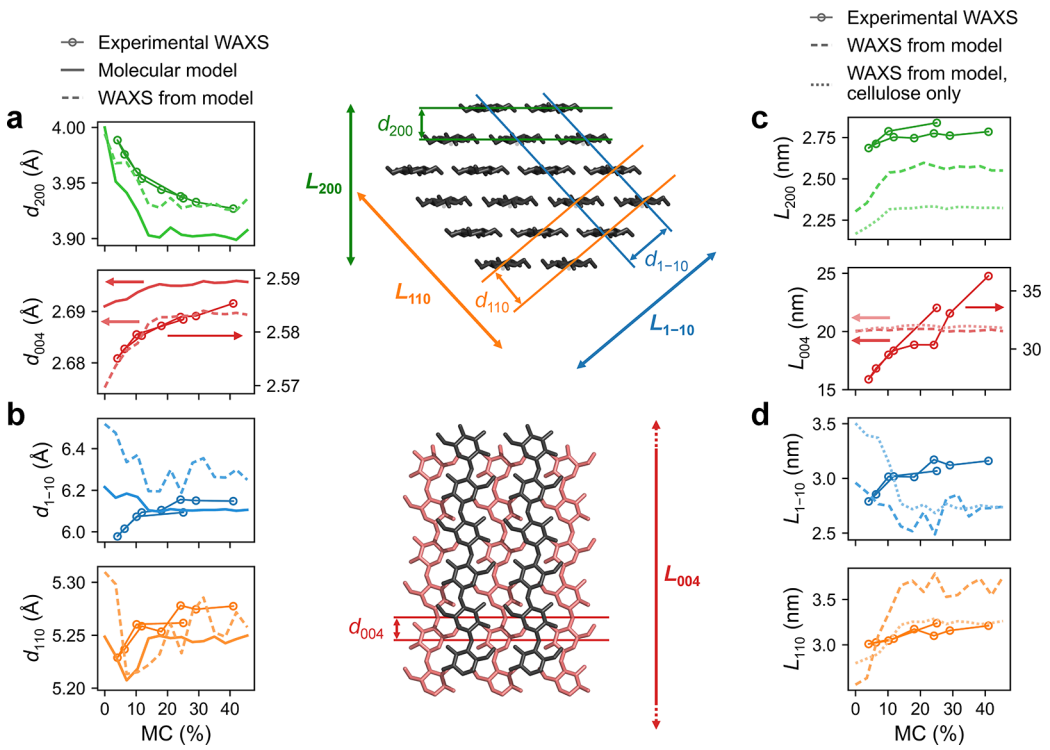

Figure 3. Moisture-dependence of the crystalline parameters based on WAXS experiments and molecular models. (a,b) Lattice spacings d_{hkl} and (c,d) crystal size L_{hkl} corresponding to different directions *hkl* in the crystal, as determined experimentally and from the periodic bundle model either directly (see Figure S4) or from computed scattering intensities. The MC for the models (MC_c) has been multiplied by 0.7 (approximate mass ratio of carbohydrates and total dry mass) to make it comparable with results from complete cell walls. The experimental values shown for the 200 peak correspond to a weighted average of a bimodal size distribution of crystallites (see SI for details). Note the separate vertical axes for experimental (right) and model-based (left) results for *hkl* = 004 in (a,c). See Figures S9, S10, and S11 for more results.

distorted close to the dry state (see, e.g., Figure 4e). It may bear some similarity to grain boundary effects in polycrystalline solids.[49] The general observation of drying-induced disorder in cellulose crystallites is in line with the results of several other studies utilizing different methods.[29,50−52]

Computed scattering intensities from the whole bundle of seven microfibrils (Figure S7d) gave additional insight into the effects of fibrillar aggregation on the WAXS data. The equatorial diffraction peaks were sensitive to the orientation of the microfibrils around their long axis, which occasionally allowed co-crystallization of neighboring fibrils with matching orientations. In particular, the 200 diffraction peak of the non-periodic bundle showed a broader and narrower contribution (Figure S12c,d). This was used as a basis for fitting the WAXS data of the 200 peak with two overlapping peaks, putatively originating from single and stacked microfibrils. Our models also exhibited limitations in the meridional scattering. The computed scattering intensities (Figures 2f, S7) successfully reproduced the 002 and 004 peaks originating from cellulose but not the contribution around the "forbidden" 003 reflection.[53] A moisture-sensitive 003 peak has been observed in experiments (e.g. Figure 2c, q = 1.9 Å^{-1}) and previously assigned to the organization of hemicelluloses.[18] As this peak was absent in all computed scattering regardless of the inclusion of hemicelluloses, it probably originates from structures that were not well presented by our models. Thus, both the aggregation of the microfibrils and the configuration of hemicelluloses on the microfibril surfaces likely affect the results of WAXS analysis of real samples, and scattering intensities computed from molecular models can help resolve these contributions. We did not notice any major effects due to microfibril twisting[54,55] when comparing the computed scattering intensities and moisture behavior of the non-periodic (twisting) and periodic (non-twisting) fibril models.

The equatorial anisotropic SAXS data (Figures 2a, S13) contains information on the lateral dimensions and packing of the microfibrils. They can be analyzed by a small-angle scattering model tailored for wood (WoodSAS model, eq S3),[22] which approximates the microfibrils as hexagonally packed cylinders. This fitting reproduced the previously reported, reversible trends:[29] a decrease in the microfibril packing distance and the cylinder scaling factor (sensitive to scattering contrast) with drying, as water withdraws from the space between the microfibrils (Figure 4a). This (de)swelling of the microfibril bundles is responsible for a large part of the dimensional changes of the cell wall, and therefore of the entire macroscopic sample.[23] At the macroscopic scale, the sample width decreased by 7% between MCs 29% and 4% (Figure S14), which is a slightly smaller change than the shrinkage of 10% in the microfibril bundles detected by SAXS over the same MC range. This difference is explained by other cell wall layers and different parts of the wood tissue restraining the macroscale swelling behavior.[36]

The molecular models successfully reproduced the experimentally observed linear swelling of the microfibril bundles above a few per cent MC with values of the fibril packing distance comparable to those from scattering experiments (Figures 4b). The bundle swelling in the models was accompanied by a decrease in hydrogen bonds between hemicelluloses and cellulose and between surface chains of

https://doi.org/10.1021/acs.nanolett.2c00822
Nano Lett. 2022, 22, 5143−5150

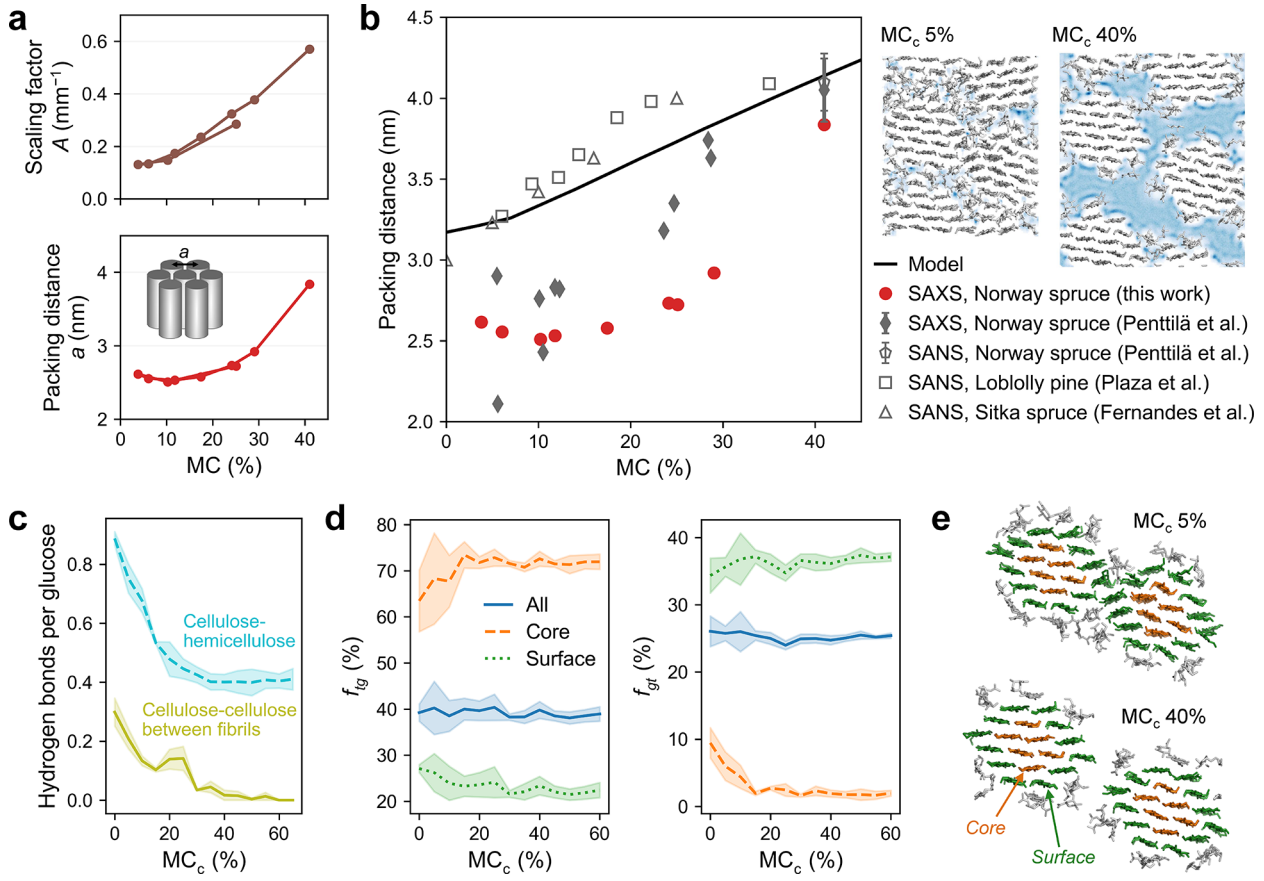

Figure 4. Moisture-related swelling of microfibril bundles based on scattering analysis and modeling. (a) Results of SAXS fits using the WoodSAS model (SI eq S3)[22] (see Figure S13 for all results). (b) Microfibril packing distance as a function of MC ($0.7 \times MC_c$) as determined from the periodic bundle model (see Figure S15 for non-periodic model) and a comparison to experimental SAXS and SANS results[20,22,23,29,58,59] (MC of 41% used for Norway spruce in water-saturated state;[39] error bars correspond to standard deviation between samples). Snapshots of the periodic model with density of water in blue are shown on the right. (c) Number of hydrogen bonds as a function of MC_c (see Figure S16 for all results). (d) Fractions (f in %) of primary alcohol group conformers (*tg, trans−gauche*; *gt, gauchetrans*) as a function of MC_c, shown separately for all cellulose chains and chains at microfibril core and surface (see Figure S17 for all results). In panels c and d, the lines correspond to the mean of all four fibrils and the filled areas to ±1 standard deviation of the means of each fibril. (e) Simulation snapshots of two microfibrils of the periodic model (cellulose in green and orange, hemicelluloses in gray), which illustrates the deformation of cellulose crystals in the dry state. This partially explains the changes in lattice spacings and experimentally determined crystal size (Figure 3).

neighboring fibrils, which are in direct contact at low MCs (Figures 4c, S16). This illustrates a close association of the hemicelluloses on the microfibril surfaces at low MCs and demonstrates the essential role of the hemicellulose matrix in absorbing water and inducing swelling of the microfibril bundles. In the computed scattering intensities, we detected a moisture-sensitive scattering contribution at the crossover region between SAXS and WAXS (q = 0.4−0.8 Å^{-1}, Figures 2e, S7), which is visible also in experimental data (Figure 2a,b). We tentatively assign this intensity increase to the hydration and reorganization of the hemicellulose shell around the microfibrils. Another indication of a reorganization of the disordered polymer matrix is the shift of the isotropic WAXS intensity maximum to lower q with drying (Figure 2a).[24]

The swelling of the microfibril bundles and reorganization of the matrix polymers have implications for the mobility of water within the bundles. As reported in a related study,[44] the diffusivity of interfibrillar water decreases rapidly with decreasing MC. This can be assigned to a reduced ability of sparsely distributed water molecules to proceed in an amorphous polysaccharide matrix.[56] The current models reproduce the exponential decrease of the diffusion coefficient of bound water as observed in ^{1}H-NMR experiments of cellulosic fibers,[57] which provides further support for the used model geometry.

Throughout the X-ray scattering and modeling results, we noticed that the changes in the SAXS and WAXS regimes, that is, at different hierarchical levels, dominated at different MC ranges. The microfibril packing distance changed mostly above MC 15% (Figure 4a), accompanied by slight changes in the microfibril orientation (Figure S18), and remained constant below it. On the contrary, the lattice spacings and the crystal size showed only small changes at high MCs and changed most significantly and with largest variations at MCs below 15% (Figure 3). A closer look into the models revealed a clear deformation of the crystals at low MCs. This manifested, among others, as an abrupt transition in the primary alcohol group conformations of the core chains from *tg* (crystalline cellulose I_β) to *gt* with decreasing MC (Figure 4d). Simultaneously, the fraction of *tg* conformers increased in the surface chains, as they occasionally adapted to the crystal structure of the neighboring fibrils (Figure 4d,e). Other works have reported abrupt changes in the mechanical properties of wood, its susceptibility to fungal degradation, and water diffusion and hydrogen bonding at

https://doi.org/10.1021/acs.nanolett.2c00822
Nano Lett. 2022, 22, 5143−5150

similar MCs,[60−62] which coincides with the softening of hemicelluloses.[3] A previous diffraction study also found the largest moisture-related changes in the lattice parameters of spruce wood cellulose below MC 13%.[33] Nevertheless, the detailed mechanisms and interactions behind these changes and the exact role of water in this structural transformation has so far remained elusive.

The results of our combined X-ray scattering experiments and MD simulations, supported by previous findings,[2,3,20,23,33,35,36] can be taken together to outline a coherent picture of the structural changes in microfibril bundles at different MC ranges (Figure 5). Even though individual pieces of this picture existed

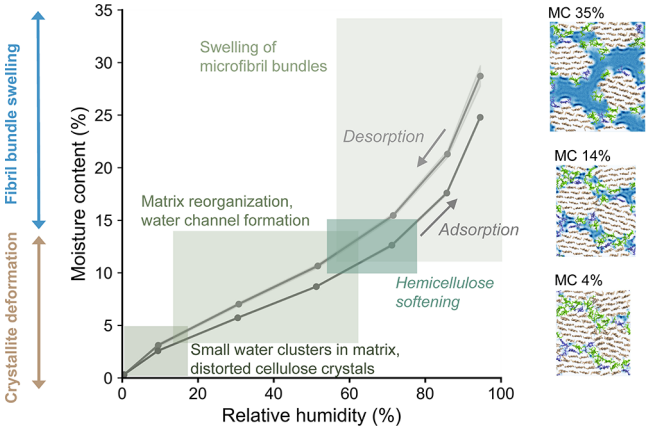

Figure 5. Summary of structural changes taking place in microfibril bundles in spruce wood cell walls at different MC ranges, illustrated in connection with a sorption isotherm (circles indicating the data points). In the dry state (MC close to 0%), the cellulose microfibrils are tightly packed and locked into a position where the cellulose crystallites are deformed due to interaction with the matrix polymers and neighboring fibril surfaces. Once some water becomes available (MC a few per cent), it penetrates the matrix and forms small clusters. Further increase of the MC allows the interfibrillar matrix to reorganize and to accommodate more water, which releases the deforming stresses on the microfibrils and allows them to adopt a higher level of crystalline order. At around MC 10−15%, the individual water clusters have grown and merged enough to occupy the spaces between the microfibrils, and the matrix softens in a process reminiscent of a glass transition. Above this point, the matrix can deform more easily, and it expands to accommodate more water in continuous channels, and the fibril bundles swell causing an increase in the microfibril packing distance and allowing faster diffusion of water. Simulation snapshots with MC referring to 0.7 × MC_c are shown on the right (see Figure S19 for all).

before, our current results, obtained by studying the same system with simulations and scattering experiments, helped to link the different aspects together to form a more complete image of this complex phenomenon. The exact mechanisms controlling the behavior, such as the transfer from one stage to the other, remain intriguing subjects for further studies for which the methodology presented here provides excellent tools. On the basis of our observations, the swelling of microfibril bundles originates from the sorption of water to the hemicelluloses and microfibril surfaces. However, fibrillar aggregation also plays an essential role in the moisture behavior, introducing deformations to the cellulose crystals closer to the dry state. Considering the inherent hierarchical structure formed by fibrillar units is therefore indispensable for understanding the structural and functional properties of materials based on plant cell walls. The new information provides means to understand and control the fundamentally important swelling of wood in the nanoscale, which enables the design of novel wood-based nanomaterials and other applications.

Our study shows clear methodological advances when combining molecular simulations and X-ray scattering for a more accurate interpretation of nanoscale interactions between water and the main structural components of plant cell walls. Our up-to-date model of microfibril bundles allowed transferring from a conceptual picture to a quantitative description of the moisture behavior of wood cell walls. It highlights the role of the hierarchical structure of the bundles, in which their deswelling eventually turns into a deformation of the cellulose crystals with continued drying. This coherent understanding forms a basis for quantitative prediction and modeling of cellulosic materials. The approach is not limited to moisture behavior of wood but can be adapted to other cellulosic nanomaterials and for studies including mechanical stresses, mechanosorption, sorption hysteresis, and irreversible effects of drying.

■ ASSOCIATED CONTENT

Supporting Information

The Supporting Information is available free of charge at https://pubs.acs.org/doi/10.1021/acs.nanolett.2c00822.

Full description on materials and methods including sample preparation, chemical analysis, X-ray scattering, X-ray microtomography, sorption experiments, and modeling; supplementary results including more detailed scattering, modeling, tomography and chemical analysis results, and a table summarizing the suggested mechanisms for cellulose lattice deformations with moisture changes (PDF)

Video of a swelling microfibril bundle based on the simulations of the periodic model with four fibrils (AVI)

■ AUTHOR INFORMATION

Corresponding Authors

Antti Paajanen − *VTT Technical Research Centre of Finland Ltd, FI-02044 Espoo, Finland*; Email: antti.paajanen@vtt.fi

Paavo A. Penttilä − *Department of Bioproducts and Biosystems, Aalto University, FI-00076 Aalto, Espoo, Finland*; orcid.org/0000-0003-0584-4918; Email: paavo.penttila@aalto.fi

Authors

Aleksi Zitting − *Department of Bioproducts and Biosystems, Aalto University, FI-00076 Aalto, Espoo, Finland*; orcid.org/0000-0003-0241-9174

Lauri Rautkari − *Department of Bioproducts and Biosystems, Aalto University, FI-00076 Aalto, Espoo, Finland*; orcid.org/0000-0002-1207-220X

Jukka A. Ketoja − *VTT Technical Research Centre of Finland Ltd, FI-02044 Espoo, Finland*; orcid.org/0000-0002-8260-4267

Complete contact information is available at: https://pubs.acs.org/10.1021/acs.nanolett.2c00822

Author Contributions

P.A.P. and A.P. conceptualized the research and applied funding with the aid of J.A.K. P.A.P. and A.Z. prepared the samples and conducted the scattering experiments. A.Z. conducted the sorption experiments. A.P. conducted the simulations, analyzed

https://doi.org/10.1021/acs.nanolett.2c00822
Nano Lett. 2022, 22, 5143−5150

the results, and computed the scattering intensities from the models. P.A.P. analyzed the experimental and simulated scattering data and wrote the manuscript with contributions from all authors. All authors involved in the interpretation of the results.

Notes

The authors declare no competing financial interest.

■ ACKNOWLEDGMENTS

This work was a part of the Academy of Finland's Flagship Programme under Project Nos. 318890 and 318891 (Competence Center for Materials Bioeconomy, FinnCERES). P.A.P. thanks the Academy of Finland for funding (Grant 315768). The authors wish to acknowledge CSC − IT Center for Science, Finland, for computational resources. This work made use of Aalto University Bioeconomy Facilities and OtaNano−Nanomicroscopy Center Facilities and used services of the University of Helsinki X-ray Micro-CT Laboratory. Thanks is given to Dr. Heikki Suhonen for conducting the X-ray microtomography experiments, Suvi Kyyrö for helping with sample preparation, Atte Mikkelson for compositional analysis, and Dr. Daniela Altgen for the illustration of a wood trunk.

■ ABBREVIATIONS

GAX, glucuronoarabinoxylan; GGM, galactoglucomannan; MC, moisture content; MC_c, moisture content relative to carbohydrates; MD, molecular dynamics; RH, relative humidity; SANS, small-angle neutron scattering; SAXS, small-angle X-ray scattering; WAXS, wide-angle X-ray scattering.

■ REFERENCES

(1) Brischke, C.; Alfredsen, G. Wood-water relationships and their role for wood susceptibility to fungal decay. *Appl. Microbiol. Biotechnol.* **2020**, *104*, 3781−3795.
(2) Engelund, E. T.; Thygesen, L. G.; Svensson, S.; Hill, C. A. S. A critical discussion of the physics of wood−water interactions. *Wood Sci. Technol.* **2013**, *47*, 141−161.
(3) Jakes, J. E.; Hunt, C. G.; Zelinka, S. L.; Ciesielski, P. N.; Plaza, N. Z. Effects of Moisture on Diffusion in Unmodified Wood Cell Walls: A Phenomenological Polymer Science Approach. *Forests* **2019**, *10*, 1084.
(4) Salmén, L.; Burgert, I. Cell wall features with regard to mechanical performance. A review COST Action E35 2004−2008: Wood machining − micromechanics and fracture. *Holzforschung* **2009**, *63*, 121−129.
(5) Thybring, E. E.; Fredriksson, M. Wood Modification as a Tool to Understand Moisture in Wood. *Forests* **2021**, *12*, 372.
(6) Berglund, L. A.; Burgert, I. Bioinspired Wood Nanotechnology for Functional Materials. *Adv. Mater.* **2018**, *30*, 1704285.
(7) Chen, C.; Kuang, Y.; Zhu, S.; Burgert, I.; Keplinger, T.; Gong, A.; Li, T.; Berglund, L.; Eichhorn, S. J.; Hu, L. Structure−property−function relationships of natural and engineered wood. *Nat. Rev. Mater.* **2020**, *5*, 642−666.
(8) Jiang, F.; Li, T.; Li, Y.; Zhang, Y.; Gong, A.; Dai, J.; Hitz, E.; Luo, W.; Hu, L. Wood-Based Nanotechnologies toward Sustainability. *Adv. Mater.* **2018**, *30*, 1703453.
(9) Kontturi, E.; Laaksonen, P.; Linder, M. B.; Nonappa; Gröschel, A. H.; Rojas, O. J.; Ikkala, O. Advanced Materials through Assembly of Nanocelluloses. *Adv. Mater.* **2018**, *30*, 1703779.
(10) Ajdary, R.; Tardy, B. L.; Mattos, B. D.; Bai, L.; Rojas, O. J. Plant Nanomaterials and Inspiration from Nature: Water Interactions and Hierarchically Structured Hydrogels. *Adv. Mater.* **2021**, *33*, 2001085.
(11) Heise, K.; Kontturi, E.; Allahverdiyeva, Y.; Tammelin, T.; Linder, M. B.; Nonappa; Ikkala, O. Nanocellulose: Recent Fundamental Advances and Emerging Biological and Biomimicking Applications. *Adv. Mater.* **2021**, *33*, 2004349.
(12) Beaumont, M.; Jusner, P.; Gierlinger, N.; King, A. W. T.; Potthast, A.; Rojas, O. J.; Rosenau, T. Unique reactivity of nanoporous cellulosic materials mediated by surface-confined water. *Nat. Commun.* **2021**, *12*, 2513.
(13) Jarvis, M. C. Structure of native cellulose microfibrils, the starting point for nanocellulose manufacture. *Philos. Trans. R. Soc., A* **2018**, *376*, 20170045.
(14) Meng, X.; Ragauskas, A. J. Recent advances in understanding the role of cellulose accessibility in enzymatic hydrolysis of lignocellulosic substrates. *Curr. Opin. Biotechnol.* **2014**, *27*, 150−158.
(15) Salmén, L. Wood Cell Wall Structure and Organisation in Relation to Mechanics. In *Plant Biomechanics*; Geitmann, A., Gril, J., Eds.; Springer International Publishing, 2018; pp 3−19.
(16) Cresswell, R.; Dupree, R.; Brown, S. P.; Pereira, C. S.; Skaf, M. S.; Sorieul, M.; Dupree, P.; Hill, S. Importance of Water in Maintaining Softwood Secondary Cell Wall Nanostructure. *Biomacromolecules* **2021**, *22*, 4669−4680.
(17) Terrett, O. M.; Lyczakowski, J. J.; Yu, L.; Iuga, D.; Franks, W. T.; Brown, S. P.; Dupree, R.; Dupree, P. Molecular architecture of softwood revealed by solid-state NMR. *Nat. Commun.* **2019**, *10*, 4978.
(18) Thomas, L. H.; Altaner, C. M.; Forsyth, V. T.; Mossou, E.; Kennedy, C. J.; Martel, A.; Jarvis, M. C. Nanostructural deformation of high-stiffness spruce wood under tension. *Sci. Rep.* **2021**, *11*, 453.
(19) Rongpipi, S.; Ye, D.; Gomez, E. D.; Gomez, E. W. Progress and Opportunities in the Characterization of Cellulose − An Important Regulator of Cell Wall Growth and Mechanics. *Front. Plant Sci.* **2019**, *9*, 1894.
(20) Fernandes, A. N.; Thomas, L. H.; Altaner, C. M.; Callow, P.; Forsyth, V. T.; Apperley, D. C.; Kennedy, C. J.; Jarvis, M. C. Nanostructure of cellulose microfibrils in spruce wood. *Proc. Natl. Acad. Sci. U. S. A.* **2011**, *108*, E1195−E1203.
(21) Jakob, H. F.; Tschegg, S. E.; Fratzl, P. Hydration Dependence of the Wood-Cell Wall Structure in *Picea abies*. A Small-Angle X-ray Scattering Study. *Macromolecules* **1996**, *29*, 8435−8440.
(22) Penttilä, P. A.; Rautkari, L.; Österberg, M.; Schweins, R. Small-angle scattering model for efficient characterization of wood nanostructure and moisture behaviour. *J. Appl. Crystallogr.* **2019**, *52*, 369−377.
(23) Plaza, N. Z.; Pingali, S. V.; Qian, S.; Heller, W. T.; Jakes, J. E. Informing the improvement of forest products durability using small angle neutron scattering. *Cellulose* **2016**, *23*, 1593−1607.
(24) Abe, K.; Yamamoto, H. Mechanical interaction between cellulose microfibril and matrix substance in wood cell wall determined by X-ray diffraction. *J. Wood Sci.* **2005**, *51*, 334−338.
(25) Agarwal, U. P.; Ralph, S. A.; Baez, C.; Reiner, R. S.; Verrill, S. P. Effect of sample moisture content on XRD-estimated cellulose crystallinity index and crystallite size. *Cellulose* **2017**, *24*, 1971−1984.
(26) Fang, L.; Catchmark, J. M. Structure characterization of native cellulose during dehydration and rehydration. *Cellulose* **2014**, *21*, 3951−3963.
(27) Hill, S. J.; Kirby, N. M.; Mudie, S. T.; Hawley, A. M.; Ingham, B.; Franich, R. A.; Newman, R. H. Effect of drying and rewetting of wood on cellulose molecular packing. *Holzforschung* **2010**, *64*, 421−427.
(28) Leppänen, K.; Bjurhager, I.; Peura, M.; Kallonen, A.; Suuronen, J.-P.; Penttilä, P.; Love, J.; Fagerstedt, K.; Serimaa, R. X-ray scattering and microtomography study on the structural changes of never-dried silver birch, European aspen and hybrid aspen during drying. *Holzforschung* **2011**, *65*, 865−873.
(29) Penttilä, P. A.; Altgen, M.; Carl, N.; van der Linden, P.; Morfin, I.; Österberg, M.; Schweins, R.; Rautkari, L. Moisture-related changes in the nanostructure of woods studied with X-ray and neutron scattering. *Cellulose* **2020**, *27*, 71−87.
(30) Salmén, L.; Stevanic, J. S.; Holmqvist, C.; Yu, S. Moisture induced straining of the cellulosic microfibril. *Cellulose* **2021**, *28*, 3347−3357.
(31) Toba, K.; Yamamoto, H.; Yoshida, M. Mechanical interaction between cellulose microfibrils and matrix substances in wood cell walls induced by repeated wet-and-dry treatment. *Cellulose* **2012**, *19*, 1405−1412.

https://doi.org/10.1021/acs.nanolett.2c00822
Nano Lett. 2022, 22, 5143−5150

(32) Yamamoto, H.; Ruelle, J.; Arakawa, Y.; Yoshida, M.; Clair, B.; Gril, J. Origin of the characteristic hygro-mechanical properties of the gelatinous layer in tension wood from Kunugi oak (*Quercus acutissima*). *Wood Sci. Technol.* **2010**, *44*, 149−163.
(33) Zabler, S.; Paris, O.; Burgert, I.; Fratzl, P. Moisture changes in the plant cell wall force cellulose crystallites to deform. *J. Struct. Biol.* **2010**, *171*, 133−141.
(34) Zhou, S.; Jin, K.; Buehler, M. J. Understanding Plant Biomass via Computational Modeling. *Adv. Mater.* **2021**, *33*, 2003206.
(35) Kulasinski, K.; Derome, D.; Carmeliet, J. Impact of hydration on the micromechanical properties of the polymer composite structure of wood investigated with atomistic simulations. *J. Mech. Phys. Solids* **2017**, *103*, 221−235.
(36) Derome, D.; Kulasinski, K.; Zhang, C.; Chen, M.; Carmeliet, J. Using Modeling to Understand the Hygromechanical and Hysteretic Behavior of the S2 Cell Wall Layer of Wood. In *Plant Biomechanics*; Geitmann, A., Gril, J., Eds.; Springer International Publishing, 2018; pp 247−269.
(37) Penttilä, P. A.; Paajanen, A.; Ketoja, J. A. Combining scattering analysis and atomistic simulation of wood-water interactions. *Carbohydr. Polym.* **2021**, *251*, 117064.
(38) Penttilä, P.; Zitting, A. X-ray scattering data from Norway spruce at different moisture conditions. *Zenodo* **2022**, DOI: 10.5281/zenodo.6557385.
(39) Thybring, E. E.; Digaitis, R.; Nord-Larsen, T.; Beck, G.; Fredriksson, M. How much water can wood cell walls hold? A triangulation approach to determine the maximum cell wall moisture content. *PLoS One* **2020**, *15*, No. e0238319.
(40) Nixon, B. T.; Mansouri, K.; Singh, A.; Du, J.; Davis, J. K.; Lee, J.-G.; Slabaugh, E.; Vandavasi, V. G.; O'Neill, H.; Roberts, E. M.; Roberts, A. W.; Yingling, Y. G.; Haigler, C. H. Comparative Structural and Computational Analysis Supports Eighteen Cellulose Synthases in the Plant Cellulose Synthesis Complex. *Sci. Rep.* **2016**, *6*, 28696.
(41) Nishiyama, Y.; Langan, P.; Chanzy, H. Crystal Structure and Hydrogen-Bonding System in Cellulose Iβ from Synchrotron X-ray and Neutron Fiber Diffraction. *J. Am. Chem. Soc.* **2002**, *124*, 9074−9082.
(42) Yang, H.; Kubicki, J. D. A density functional theory study on the shape of the primary cellulose microfibril in plants: effects of C6 exocyclic group conformation and H-bonding. *Cellulose* **2020**, *27*, 2389−2402.
(43) Nishiyama, Y.; Kim, U.-J.; Kim, D.-Y.; Katsumata, K. S.; May, R. P.; Langan, P. Periodic Disorder along Ramie Cellulose Microfibrils. *Biomacromolecules* **2003**, *4*, 1013−1017.
(44) Zitting, A.; Paajanen, A.; Rautkari, L.; Penttilä, P. A. Deswelling of microfibril bundles in drying wood studied by small-angle neutron scattering and molecular dynamics. *Cellulose* **2021**, *28*, 10765−10776.
(45) Zhang, Y.; Inouye, H.; Crowley, M.; Yu, L.; Kaeli, D.; Makowski, L. Diffraction pattern simulation of cellulose fibrils using distributed and quantized pair distances. *J. Appl. Crystallogr.* **2016**, *49*, 2244−2248.
(46) Dri, F. L.; Wu, X.; Moon, R. J.; Martini, A.; Zavattieri, P. D. Evaluation of reactive force fields for prediction of the thermo-mechanical properties of cellulose I$_\beta$. *Comput. Mater. Sci.* **2015**, *109*, 330−340.
(47) Daicho, K.; Kobayashi, K.; Fujisawa, S.; Saito, T. Recovery of the Irreversible Crystallinity of Nanocellulose by Crystallite Fusion: A Strategy for Achieving Efficient Energy Transfers in Sustainable Biopolymer Skeletons. *Angew. Chem. Int. Ed.* **2021**, *60*, 24630−24636.
(48) Abe, K.; Yamamoto, H. Change in mechanical interaction between cellulose microfibril and matrix substance in wood cell wall induced by hygrothermal treatment. *J. Wood Sci.* **2006**, *52*, 107−110.
(49) Gleiter, H. Nanocrystalline materials. *Prog. Mater. Sci.* **1989**, *33*, 223−315.
(50) Agarwal, U. P. 1064 nm FT-Raman spectroscopy for investigations of plant cell walls and other biomass materials. *Front. Plant Sci.* **2014**, *5*, 490.
(51) Hirai, A.; Horii, F.; Kitamaru, R. Solid-State High-Resolution Carbon-13 NMR Studies of Celluloses. *Bull. Inst. Chem. Res. Kyoto Univ.* **1986**, *63*, 340−359.
(52) Park, S.; Johnson, D. K.; Ishizawa, C. I.; Parilla, P. A.; Davis, M. F. Measuring the crystallinity index of cellulose by solid state ^{13}C nuclear magnetic resonance. *Cellulose* **2009**, *16*, 641−647.
(53) French, A. D. Idealized powder diffraction patterns for cellulose polymorphs. *Cellulose* **2014**, *21*, 885−896.
(54) Ogawa, Y. Electron microdiffraction reveals the nanoscale twist geometry of cellulose nanocrystals. *Nanoscale* **2019**, *11*, 21767−21774.
(55) Paajanen, A.; Ceccherini, S.; Maloney, T.; Ketoja, J. A. Chirality and bound water in the hierarchical cellulose structure. *Cellulose* **2019**, *26*, 5877−5892.
(56) Kulasinski, K.; Guyer, R.; Derome, D.; Carmeliet, J. Water Diffusion in Amorphous Hydrophilic Systems: A Stop and Go Process. *Langmuir* **2015**, *31*, 10843−10849.
(57) Topgaard, D.; Söderman, O. Diffusion of Water Absorbed in Cellulose Fibers Studied with ^{1}H-NMR. *Langmuir* **2001**, *17*, 2694−2702.
(58) Penttilä, P. A.; Altgen, M.; Awais, M.; Österberg, M.; Rautkari, L.; Schweins, R. Bundling of cellulose microfibrils in native and polyethylene glycol-containing wood cell walls revealed by small-angle neutron scattering. *Sci. Rep.* **2020**, *10*, 20844.
(59) Penttilä, P. A.; Zitting, A.; Lourençon, T.; Altgen, M.; Schweins, R.; Rautkari, L. Water-accessibility of interfibrillar spaces in spruce wood cell walls. *Cellulose* **2021**, *28*, 11231−11245.
(60) Guo, X.; Qing, Y.; Wu, Y.; Wu, Q. Molecular association of adsorbed water with lignocellulosic materials examined by micro-FTIR spectroscopy. *Int. J. Biol. Macromol.* **2016**, *83*, 117−125.
(61) Plaza, N. Z. On the Experimental Assessment of the Molecular-Scale Interactions between Wood and Water. *Forests* **2019**, *10*, 616.
(62) Thybring, E. E.; Glass, S. V.; Zelinka, S. L. Kinetics of Water Vapor Sorption in Wood Cell Walls: State of the Art and Research Needs. *Forests* **2019**, *10*, 704.

https://doi.org/10.1021/acs.nanolett.2c00822
Nano Lett. 2022, 22, 5143−5150